Neutron Scattering Study and Dynamic Properties of Hydrogen-Bonded Liquids in Mesoscopic Confinement. 1. The Water Case†

V. Crupi, D. Majolino, P. Migliardo,* and V. Venuti

Dipartimento di Fisica dell'Università di Messina and INFM Sezione di Messina, C.da Papardo, S.ta Sperone 31, P. O. Box 55, 98166 S. Agata, Messina, Italy

Received: February 22, 2002; In Final Form: July 8, 2002

In the present work we report a detailed spectroscopic analysis of diffusive relaxation and vibrational properties of water in bulk and confined in nanopores of Gelsil glass, at different temperatures and different hydration percentages, performed by incoherent quasi-elastic and inelastic neutron scattering, IQENS and IINS, respectively. IQENS spectra are analyzed in the framework of two different models: the confined diffusion model (CDM) and the relaxing cage model (RCM). The first one is based on the well-known random jump diffusion model for confined diffusion; the second one takes into account the α-relaxation dynamics predicted by mode coupling theory (MCT) of supercooled liquids. Finally, the analysis of IINS spectra has been addressed to the comprehension of the evolution of the one-phonon-amplitude weighted proton vibrational density of states (VDOS), $Z(\omega)$, when the water loses its peculiar bulk properties and originates a new structural environment due to its surface interaction.

I. Introduction

In recent years a considerable amount of interest has been devoted to the investigation of the modification, relative to the bulk state, of the structural and dynamic properties of liquid water under the constraints of spatial restrictions, in order to understand the confinement and interfacial effects on the physical behavior of this peculiar liquid.[1−3] Generally speaking, two competing effects seem to play the main role in modifying the dynamics of confined water with respect to the bulk state: the interaction forces with the substrate molecules (chemical traps), and the bare geometrical confinement (physical traps), i.e., the excluded volume effect. The separation of these two contributions, whose interplay is strongly dependent on the particle density and the size of the confining system, is still a problem that has not been completely solved yet.[4−6]

In the past decade, many studies of the structural and dynamic properties of water in different spatially restricted environments have been published. Structural studies on heavy water confined in a variety of systems, either hydrophobic or hydrophilic, whose pore dimension ranged from 50 Å to several hundreds of angstroms, have been published.[7−9] The diffusive dynamics has been mostly studied by NMR[10] and quasi-elastic neutron scattering,[11,12] both of which reveal a slowing down of the translational motion compared to bulk water. Furthermore, there are many neutron and light scattering experiments aimed at extracting relevant information on the dynamic structure factor. There are also a number of computer simulation studies on the mobility of water confined in nanopores.[13−15] Generally speaking, experimental techniques and theoretical approaches have shown that there are two types of water in the confining pores, namely "free water", which is in the middle of the pore, and "bound water", which instead is close to the wall. It was observed that free water tends to freeze abruptly in the cubic ice structure, while bound water freezes gradually without forming ice. Layering effects of water close to the walls have been shown under varying confinement conditions.

As far as modified structural properties of such a liquid in a confined environment are concerned, experimental results from neutron diffraction for heavy water in two high surface area silica samples, Spherisorb (90 Å) and Gelsil (20 Å), have been presented by Dore and co-workers.[16] In this paper the authors showed that the structural molecular arrangement is very similar to that of bulk liquid and that the modification due to the substrate is restricted to a region within 10 Å or less from the interface (see Figure 6 in ref 16).

Recently, Gallo et al.[17] presented results of molecular dynamics simulation of SPC/E water confined in a silica pore. They showed the dependence of microscopic structural and dynamic properties on the degree of hydration of the pores. In particular, the authors revealed the occurrence that two quite distinct subsets of water molecules are detectable. Those belonging to the first layer close to the substrate suffer from a severe slowing down, while the other subsets show a behavior that is typical of supercooled liquids.

Concerning dynamic properties, our research group presented a detailed analysis of Rayleigh wing and Raman scattering data performed in water confined in a nanoporous GelSil matrix.[18] We showed that the confinement of water strongly influences both the low-frequency quasi-elastic and inelastic contributions and the fundamental intramolecular OH stretching mode region. As far as Rayleigh wing data are concerned, the formation of transient extended structures, due to the presence of hydrogen bonds, gives rise to a distribution of relaxation times for reorientational motions, well described by a Havriliak−Negami profile, that plays, in the ω-domain, the same role as the KWW-$(t) = \exp[-(t/\tau_{KWW})^{\beta}]$ function in the time domain. This latter, as is well-known, seems to be the universal function obeyed by slow relaxations occurring in complex condensed systems. In the restricted translational region the results show a strong

† Preliminary results of the present work have been presented at the International Conference on Neutron Scattering, ICNS, 2001 (München, Germany), and at the International Conference LANMAT, 2001 (Venice, Italy).

* Corresponding author. Telephone: +39 090 391478. Fax: +39 090 395004. E-mail: migliard@dsme01.messina.infm.it.

10.1021/jp020503m CCC: $22.00
Published on Web 09/28/2002

modification of the vibrational dynamics of water in the confined state, with the disappearance of the 60 and 170 cm^{-1} lattice bands in the effective Raman vibrational density of states (VDOS). Furthermore, the collective contribution to the polarized OH stretching band diminishes when the hydration percentage of water in the pores decreases.

An extensive analysis of single-particle dynamics of water molecules confined in nanopores of Vycor glass has been carried out by Bellissent-Funel et al.[12,19] using incoherent quasi-elastic and inelastic neutron scattering. They found that the translational relaxation times, in the framework of the Dianoux−Volino model for confined diffusion,[20] are longer with respect to the bulk case. Furthermore, the proton density of states for confined water shows a shift in the translational and librational modes to higher frequencies, indicating a hindrance of the intermolecular motions of water molecules close to the hydrophilic surface. In a subsequent paper,[19] the authors verified that it is possible to treat the incoherent quasi-elastic neutron scattering (IQENS) spectral intensity from interfacial water as being a single quasi-elastic peak arising from a nonexponential relaxation. The origin of the nonexponential form of the incoherent structure factor is linked to the diffusion process of the water molecules that is strongly coupled to the local structural relaxation of neighboring shells and controlled by itself. This relaxation is also called the cage effect and is discussed extensively in the literature dealing with mode coupling theory of supercooled liquids.[21]

In the present paper we report on the results of a detailed analysis performed by incoherent quasi-elastic and inelastic neutron scattering in water, in the bulk state and confined into a sol−gel porous glass with 26 Å diameter pores, at different hydration levels and different temperatures. This study allowed us to get a better insight into the complex and interesting scenario of confined water, whose low-frequency dynamics is strongly modified by specific interaction with the surface (in our case hydrogen bonding between the H_2O molecules and the SiOH groups present on the inner surface of the pores). Preliminary data, in the case of bulk and fully hydrated confined water (100% of coverage) at room temperature ($T = 20$ °C), have already been presented.[22] The IQENS experimental results have been interpreted in terms of two different models: the confined diffusion model (CDM) and the relaxing cage model (RCM). The CDM is based on the well-known Volino−Dianoux model for confined diffusion, while the RCM uses an idea borrowed from mode coupling theory (MCT). This latter is based on the *cage effect* present in the liquid state, which can be seen as a transient trapping of molecules by their neighbors because of the lowering of temperature. The cage can be due to the distorted tetrahedral H-bond, formed by the neighboring environments, which tends to grow when T decreases, giving rise to a transient gel network whose lifetime is imposed by the finite H-bond lifetime (∼1 ps at $T = 20$ °C). In particular, the fit of the quasi-elastic spectra in the CDM case has been performed by a weighted superposition of an elastic (δ-function) and two quasi-elastic (Lorentzian in character) central peaks. From the behavior of the line width Γ_{tr} vs Q for the translational Lorentzian contribution, we obtained the dimension of the diffusing region $d^* = 2\pi/Q^*$ that is comparable to the one obtained by the fitting procedure of the EISF (elastic incoherent structure factor) intensity vs Q, and whose trend, as a function of temperature and hydration percentage, will be shown and explained in the following sections. In the framework of the RCM model, the quasi-elastic structure factor has been well fitted by the Havriliak−Negami function, whose relevant fitting parameters furnished the mean relaxation time $\langle\tau\rangle$ and the width of the distribution β, both Q-dependent. $\langle\tau\rangle$ showed a power-law dependence on Q, with an exponent less than 2, reflecting the nonhydrodynamic behavior of water diffusion in confinement conditions. Furthermore, β is definitively less than 1 and increases when Q diminishes.

As far as incoherent inelastic neutron scattering (IINS) spectra are concerned, we focused our analysis on the low-frequency, low-symmetry, collective vibrational properties of water molecules at various degrees of hydration, which are very sensitive to perturbative effect (anharmonicity) induced by water−surface dipole−dipole interaction. From the analysis of the spectra, in the case of confined water, a flattening and attenuation of the hindered translational modes at ∼8 and ∼20 meV and an enhancement of that librational mode centered at ∼91 meV, connected with the H_2O molecules H-bonded with the pore surface, are clearly evident.

In the next section a detailed analysis of the incoherent quasi-elastic neutron scattering (IQENS) and incoherent inelastic neutron scattering (IINS) spectral features for confined water will be presented. The high quality of the spectra will allow us to confirm the spectral behavior anticipated in ref 22, that surface water loses its peculiar bulk properties and initiates different structural environments due to surface interactions, driven by H-bonding, in which the vibrational dynamics of water tends to localize and the diffusive processes tend to freeze.

II. Experimental Section and Data Reduction

We have performed incoherent quasi-elastic neutron scattering (IQENS) and incoherent inelastic neutron scattering (IINS) measurements on water in bulk and in the confined state, at temperatures $T = -35$, -12, 20, and 40 °C and different hydration percentages $N/N_0 = 100\%$, 95%, and 5%. We have chosen these percentage values because the first one (100%) corresponds to fully hydrated water within the pores which are totally loaded, the second one (95%) represents the water that loses its bulk properties (see Figures 3 and 5 of ref 18), and the last one (5%) corresponds to tightly hydrated water on the first shell only.

As confining matrix we used Gelsil porous glass,[23] cylindrical in shape (5 mm diameter, 2 mm thickness), produced by sol−gel technology and purchased from Geltech Co., with nominal pore diameter 26 Å (5% standard deviation), pore volume fraction 0.39, glass surface area 609 m^2/g, and bulk density 1.2 g/cm^3. The pores in the glass are highly branched and connected in a fractal-like geometry. A great number of Si−OH groups, strong active sites for the interaction with water, is present on the inner pore surface, allowing the existence also of double H-bonding between surface and absorbed water. We used the following procedure for the preparation of the porous glass: the Gelsil disks were immersed in 30% hydrogen peroxide and heated to 90 °C for a few hours to remove any organic impurities absorbed by the glass. They were then washed several times in distilled water to remove the hydrogen peroxide and stored in distilled water. Successively the porous glass disks were pumped under vacuum at sufficiently high temperature (∼90 °C). In such a way, the Gelsil glass becomes a translucent and clear "dry" glass. A fully hydrated Gelsil glass adsorbs water up to 25% of its dry weight. The partially hydrated samples have been obtained by drying a fully hydrated one until the desired level of hydration is reached. The water content was determined by

$$\left(\frac{\text{wt of water} \times 100}{\text{wt of dry Gelsil}}\right)\% = \%\ \text{regain}$$

On the basis of the previously described characteristic parameters of our glasses, we can conclude that the data taken for $N/N_0 = 5\%$ refer to water bonded to the inner glass surface only in the first layer.

The quasi-elastic and inelastic neutron scattering experiments were performed on the focusing time-of-flight (tof) spectrometer IN6 at Institut Laue-Langevin (ILL) in Grenoble. The instrumental conditions were chosen in such a way as to achieve a good energy resolution at Q values less than 2 Å^{-1}. The incident neutron wavelength was $\lambda_0 = 5.12$ Å, the elastic energy resolution (fwhm) was 100 μeV, determined with a vanadium standard, and the momentum range was from 0.283 to 1.9375 Å^{-1}. We performed measurements as a function of temperature in the range +40 to −35 °C, by using a cryogenic apparatus furnished by ILL that allows a temperature stabilization within ±0.1 °C in the entire explored range. To have a good signal in the neutron scattering process, we used an array of six porous cylinders fitted within an aluminum circular sheet sealed in a cylindrical sample holder. Because of the very high spectral efficiency of the IN6 tof spectrometer, an acquisition time of up to 8 h (for the sample with the lowest hydration level $N/N_0 = 5\%$) was enough to obtain spectra with good signal-to-noise ratio.

The data have been corrected for the empty cell, sample absorption, and detector efficiency, and then transformed to energy scale using standard programs available at ILL.

III. Results and Discussion

(a) IQENS Measurements. It is well-known that the main contribution to the scattering cross section for liquid water is the incoherent scattering by protons. In the Born approximation for N identical nuclei (H in our case),[24] the cross section is proportional to the incoherent structure factor $S_{inc}(\mathbf{Q},\omega)$. This latter turns out to be the Fourier transform of the Van Hove self-correlation function $G_s(\mathbf{r},t)$, which in the case of translationally invariant systems is a function of the scalar distance r and time t. In the quasi-elastic region the $S_{inc}(\mathbf{Q},\omega)$ is written as

$$S_{inc}(\mathbf{Q},\omega) = T_{inc}(\mathbf{Q},\omega) \otimes R_{inc}(\mathbf{Q},\omega) \otimes V_{inc}(\mathbf{Q},\omega) \quad (1)$$

where $T_{inc}(\mathbf{Q},\omega)$ represents the translational center of mass local motion contribution, $R_{inc}(\mathbf{Q},\omega)$ represents the rotational motion of the protons relative to center of mass, and finally $V_{inc}(\mathbf{Q},\omega)$ is the fast vibrational motion of the protons, around the mean position. In the quasi-elastic region $V_{inc}(\mathbf{Q},\omega)$ is the Debye−Waller term. Historically speaking, under the assumption of weak coupling among these motions and an isotropic rotational diffusion motion around the center of mass of the water molecule, we obtain the following equation as a good theoretical scattering function, valid for bulk isotropic fluids:

$$S_s(Q,\omega) = e^{-Q^2\langle u^2\rangle/3}\left\{ J_0^2(Qa)\frac{1}{\pi}\frac{\Gamma_{tr}(Q)}{(\Gamma_{tr}(Q))^2+\omega^2} + \sum_{l=1}^{\infty}(2l+1)J_l^2(Qa)\frac{1}{\pi}\frac{\Gamma_{tr}(Q)+l(l+1)D_{rot}}{[\Gamma_{tr}(Q)+l(l+1)D_{rot}]^2+\omega^2}\right\} \quad (2)$$

where J_l are the spherical Bessel functions, D_{rot} is the rotational diffusion coefficient, Γ_{tr} is the translational line width, and a is the O−H distance (in our case $a \cong 0.98$ Å). For confined liquids, the shape of IQENS spectra is strongly modified due to the broken translational symmetry as a consequence of geometric confinement. In this case, following the model first developed by Volino and Dianoux,[20,25,26] the scattering law in the CDM case becomes

$$S_s(Q,\omega) = e^{-Q^2\langle u^2\rangle/3}\{A(Q)\,\delta(\omega) + (1-A(Q))[L_{tr}(Q,\omega) + L_{rot}(Q,\omega)]\} \otimes R(Q,\omega) + \text{bkg} \quad (3)$$

i.e., the spectral line shape is the weighted superposition of an elastic (δ-function) and two quasi-elastic peaks Lorentzian in character, $L_{tr}(Q,\omega)$ and $L_{rot}(Q,\omega)$, taking into account the translational and rotational motions, respectively; bkg is a flat background. $A(Q)$ is the elastic incoherent structure factor (EISF) for the confined protons, which turns out to be

$$A(Q) = \left[\frac{mJ_1(Qd)}{Qd}\right]^2 \quad (4)$$

where m can be 2 or 3 depending on the cylindrical or spherical diffusion volume[26] and d is the confining cage dimension. The water molecules diffuse through the interconnected pores ($m = 3$), so we have a diffusion inside a volume with an anisotropic shape, such as cylinders, having a height L (unknown in our case) and a cross-sectional radius a. In this case it is possible to observe a broader peak of the EISF term with considerable enhanced Q tail and a larger range in Q where Γ_{tr} is constant.

In Figure 1 we report the neutron scattered intensity for water in bulk and in the confined state at all the analyzed hydration percentages N/N_0, for $Q = 0.946$ Å^{-1} and $T = 20$ °C, as an example, together with the total best fit and the single components. We used eq 2 to best fit bulk water and eq 3 for confined water. In this last case it has to be noticed, as expected, that the EISF contribution (filled area in Figure 1) is quite relevant.

From the fit analysis we obtained the half-width at half-maximum of the translational Lorentzian contribution, Γ_{tr}, vs Q, shown in Figure 2 in the case of bulk water at $T = 20$ °C and $T = 40$ °C (A) and, as an example, for confined water at $N/N_0 = 100\%$ for all the analyzed temperatures (B). All the relevant results from the fitting procedure are reported in Table 1.

In the case of bulk water, the values of the self-diffusion coefficient at $T = 20$ °C and $T = 40$ °C are quite similar to those reported in the literature.[25]

CDM Model. As far as the confined state is concerned, Γ_{tr} exhibits, at all the analyzed temperatures, a Q dependence typically observed in confinement conditions: in particular, at low Q, the noteworthy result is the flattening to a constant value Γ_0 that suggests the confinement effect for water molecules inside a restricted spatial region. A first indication of the size of this region, d^*, can be calculated from the inverse of the wavevector Q^* at which the plateau is reached: $d^* = 2\pi Q^{*-1}$. As can be seen from the obtained values, all reported in Table 1, the trend of d^* is to stay less than or equal to the pore diameter and to decrease as the temperature decreases, indicating that at lower temperatures the confinement effects are enhanced. For Q values higher than Q^*, Γ_{tr} tends to restore the bulk diffusion behavior. We observed, in fact, a typical random jump diffusion that allowed us to obtain information on the diffusional dynamics inside the confinement region, since the effect of the boundary

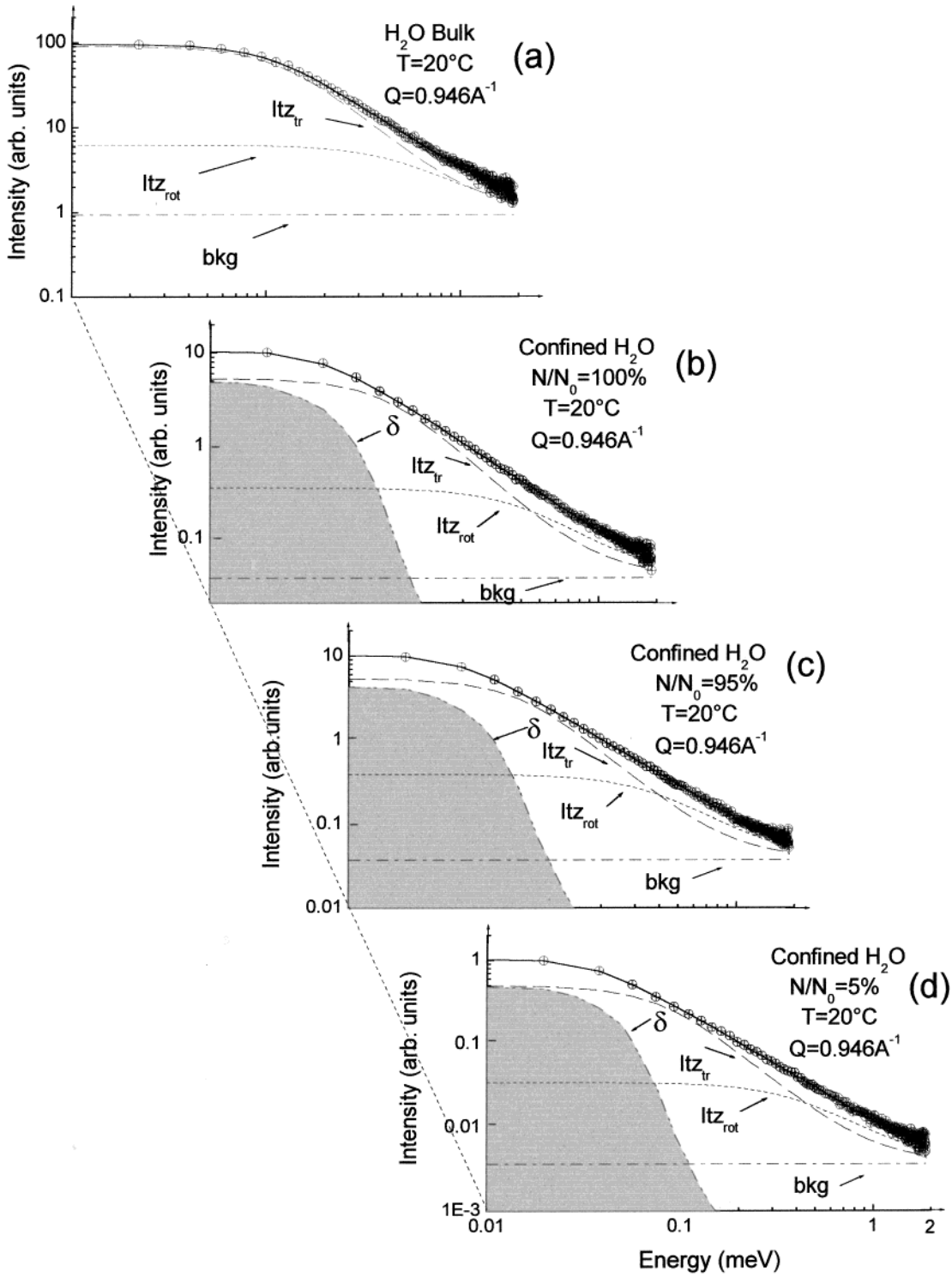

Figure 1. Experimental IQENS spectra of water in bulk (a) and in confined state at all the analyzed hydration percentages $N/N_0 = 100\%$ (b), 95% (c), and 5% (d), at $Q = 0.946$ Å^{-1} and $T = 20$ °C, together with the total best-fit and the single components. We used eq 2 to best fit bulk water and eq 3 for confined water, following the confined diffusion model, CDM. Filled area refers to the δ contribution (EISF).

is negligible. The evaluated translational diffusion coefficients are also reported in Table 1. By comparing these values with those obtained in the case of bulk water, one finds that there is a clear slowing down of the water molecule motion. Another procedure to obtain the dimension of the diffusing region is the fitting of the EISF term (see Figure 3), which we performed by using eq 4. The obtained values of d^*(EISF), as can be seen from an inspection of Table 1, follow the same trend of d^* as obtained from Γ_{tr}. The terms δ_w and δ_p are the contributions to the EISF coming from the confined water and the glass pores, respectively. This latter, coming from the vitreous matrix of the pores, is constant in all the explored Q range. It has to be noticed that in Table 1 the values of d^* are definitively lower than the geometric confining dimension (26 Å), tending to reach this value at high temperatures. This occurrence can be justified if one thinks that the shape of the pores is cylindrical and not spherical, thus inducing a higher value of the transition point Q^*. On the other hand, the T dependence of d^* is explained in terms of frozen-in effect of the diffusive proton dynamics, which is enhanced when T diminishes.

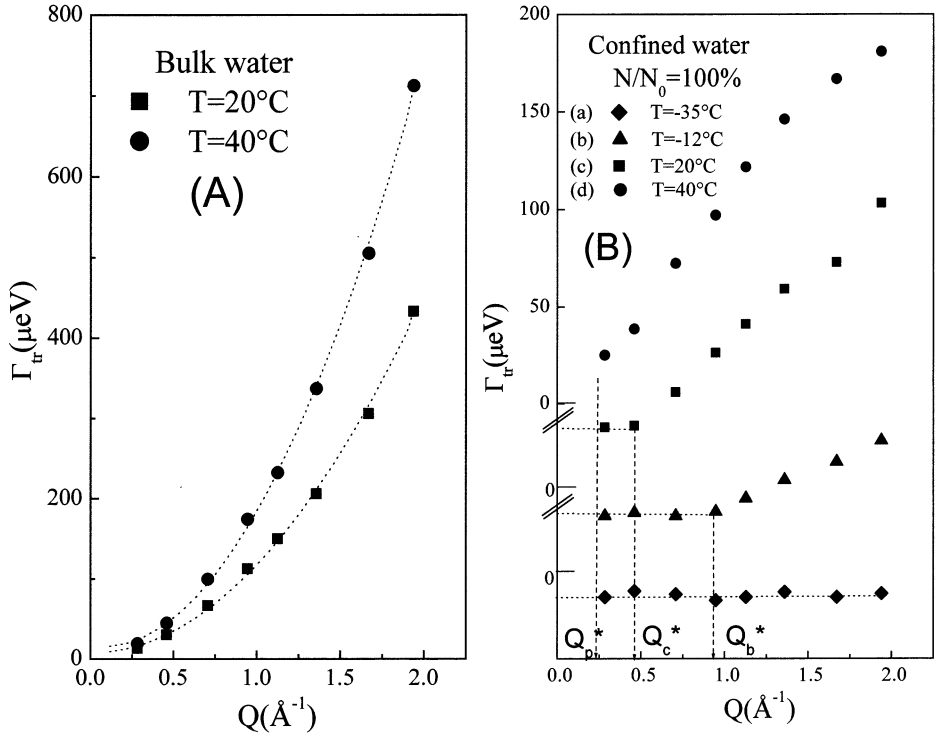

Figure 2. Translational Lorentzian contribution, Γ_{tr}, vs Q, for water in bulk (A) and confined (B) state, $N/N_0 = 100\%$, in the analyzed temperature range. In (A) the dashed curves represent the best fit following the random jump diffusion model. In (B) Q^* is referred to pore diameter.

TABLE 1: Relevant Parameters Obtained from the Fitting Procedure in the Case of CDM, for Water in Bulk and Confined State at All the Analyzed Hydration Levels and Temperatures

			confined water									
	bulk water		$N/N_0 = 100\%$				$N/N_0 = 95\%$			$N/N_0 = 5\%$		
	$T =$ 20 °C	$T =$ 40 °C	$T =$ −35 °C	$T =$ −12 °C	$T =$ 20 °C	$T =$ 40 °C	$T =$ −12 °C	$T =$ 20 °C	$T =$ 40 °C	$T =$ −12 °C	$T =$ 20 °C	$T =$ 40 °C
D^a (10^{-5} c m^2/s)	2.5	3.2		0.70	1.90	3.10	0.80	1.70	2.30	0.90	1.50	1.90
$Q^*(\Gamma_{tr})$ (Å^{-1})				0.95	0.45	0.24 (Q^*_p)	0.95	0.42	0.24 (Q^*_p)	0.95	0.39	0.24 (Q^*_p)
$d^*(\Gamma_{tr})$ (Å)				6.60	13.9	26 (d^*_p)	6.60	14.90	26 (d^*_p)	6.60	16.10	26 (d^*_p)
Q^*(EISF) (Å^{-1})			1.42	0.62	0.44	0.39	0.67	0.48	0.37	0.66	0.39	0.36
d^*(EISF) (Å)			4.40	10.10	14.30	16.10	9.40	13.10	17.0	9.50	16.10	17.40

[a] Estimated uncertainty on D is ±0.1.

As far as the rotational Lorentzian contribution is concerned, in Table 2 we summarize the Γ_{rot} values extracted from our QENS experiments, together with the rotational relaxation times τ_{rot}. These turn out to be independent of Q, as they should be. From an inspection of Table 2 it is evident that the rotational relaxation time does not show any substantial slowing down upon confinement and remains nearly the same for bulk and confined water. On the other hand, the translational contribution disappears at the lowest temperature ($T = -35$ °C), indicating a strong frozen-in effect. This different behavior between the translational and rotational diffusion could be due to a decoupling effect of these two motions.[27] As a matter of fact, whereas at sufficiently high temperatures a glass-forming liquid shows a single relaxation peak indicating that only one relaxation mechanism triggers τ_{tr}, τ_{rot}, and τ_η (viscosity relaxation time), at moderately supercooled regime, under the melting point the peak spreads into slow (α) and fast (β) relaxations. Furthermore, the latter displays an Arrhenius behavior vs T, whereas the former exhibits a non-Arrhenius behavior vs T and disappears at T_g, indicating that this slowing down is connected to the growth of distinct relaxing domains (correlated to the HB cage in the water case).

RCM Model. The diffusion process of the water molecule is coupled strongly to and is controlled by the local structural relaxation of neighboring shells or "cage effect". As a consequence, the incoherent structure factor, reflecting such a diffusion process, will assume a nonexponential form:

$$F_s(Q,t) = A(Q)\exp\left[-\left(\frac{t}{\tau}\right)^{\beta}\right] \tag{5}$$

According to this relaxing cage model (RCM), there is no purely elastic line for a supercooled bulk water or an interfacial water.

In the framework of the RCM suggestion, the IQENS spectrum for confined water can be fitted by the law

$$S_s(Q,\omega) = [\mathrm{HN}(\omega)] \otimes \mathrm{Re}\, s(\omega) + \mathrm{bkg} \tag{6}$$

In eq 6 HN(ω) represents the Havriliak−Negami distribution function:

$$\mathrm{HN}(\omega) = -(1/\omega)\,\mathrm{Im}[1 + (i\omega\tau_{HN})^{\alpha}]^{-\gamma} \tag{7}$$

which reflects the presence of a distribution of relaxation times.

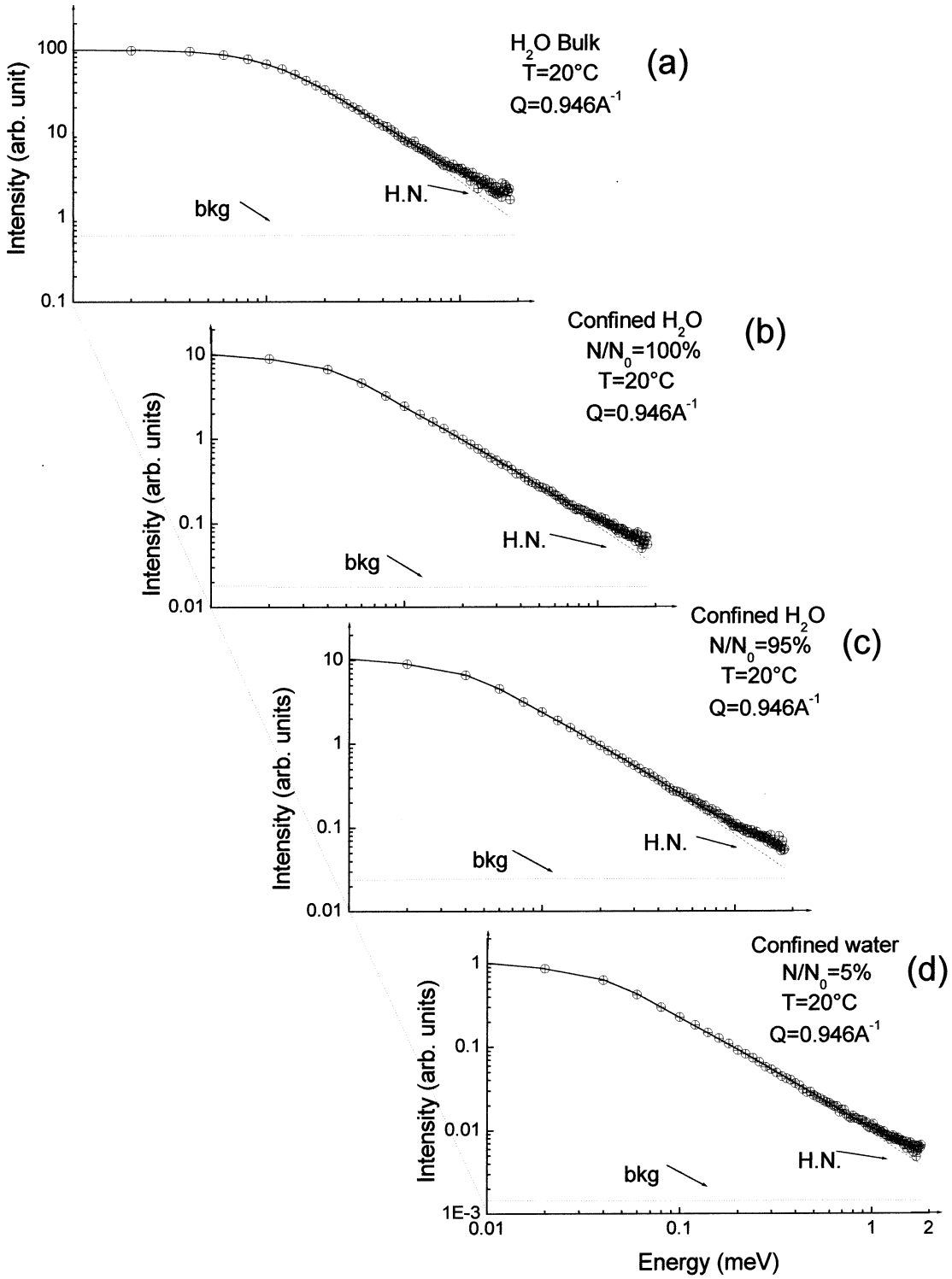

Figure 3. EISF term for confined water as obtained by CDM, at all the analyzed hydration percentages, $N/N_0 = 5\%$ (A), 95% (B), and 100% (C), and at all the studied temperatures; δ_w and δ_p represent the contributions to the EISF coming from the confined water and the glass pores, respectively. The continuous lines are the best fit by eq 4.

τ_{HN} is a characteristic relaxation time; α and γ are shape parameters ranging between 0 and 1 that are related to the symmetric (α) and asymmetric (γ) line widths.[28] Such a function plays, in the ω-domain, the same role as the well-known Kolrausch−Williams−Watt KWW(t) profile

$$\mathrm{KWW}(t) = \exp\left[-\left(\frac{t}{\tau_{\mathrm{KWW}}}\right)^{\beta}\right] \tag{8}$$

in the time domain.

In the literature, a mathematical relation between the relevant parameters of the HN(ω) and KWW(t) has been found and experimentally verified:

$$\log[\tau_{\mathrm{HN}}/\tau_{\mathrm{KWW}}] = 2.6(1-\beta)^{0.5}\exp(-3\beta) \tag{9}$$

as far as the characteristic time is concerned, and

$$\alpha\gamma = \beta^{1.23} \tag{10}$$

for the shape parameters.

TABLE 2: Half-Width at Half-Maximum of the Rotational Lorentzian Contribution, Γ_{rot}, and the Rotational Relaxation Time, τ_{rot}

			confined water					
	bulk water		$N/N_0 = 100\%$		$N/N_0 = 95\%$		$N/N_0 = 5\%$	
T (°C)	Γ_{rot} (meV)	τ_{rot} (ps)	Γ_{rot} (meV)	τ_{rot} (ps)	Γ_{rot} (meV)	τ_{rot} (ps)	Γ_{rot} (meV)	τ_{rot} (ps)
−35			0.37	1.8	0.37	1.8	0.37	1.8
−12			0.36	1.8	0.38	1.7	0.38	1.7
20	0.54	1.2	0.44	1.5	0.40	1.6	0.44	1.5
40	0.60	1.1	0.49	1.3	0.48	1.3	0.47	1.4

TABLE 3: Relevant Parameters Obtained from the Fitting Procedure in the Case of CDM, for Water in Bulk and Confined State at All the Analyzed Hydration Levels and Temperatures[a]

	$T = -12$ °C		$T = 20$ °C		$T = 40$ °C	
Q (Å^{-1})	$\langle\tau\rangle$ (ps)	b	$\langle\tau\rangle$ (ps)	b	$\langle\tau\rangle$ (ps)	b
			Bulk Water			
0.28			61.0	0.75	45.0	0.90
0.46			25.0	0.75	15.5	0.75
0.71			11.0	0.70	6.5	0.75
0.95			6.0	0.70	3.5	0.70
1.13			4.5	0.60	2.5	0.75
1.36			3.0	0.65	1.5	0.65
1.67			1.5	0.65	1.0	0.65
1.94			1.0	0.55	0.5	0.65
			Confined Water, $N/N_0 = 100\%$			
0.28	85.0	0.80	60.0	0.65	53.5	0.75
0.46	73.5	0.70	49.0	0.65	25.5	0.65
0.71	30.5	0.80	21.0	0.60	11.5	0.60
0.95	23.0	0.70	9.5	0.65	5.5	0.55
1.13	22.0	0.70	6.5	0.65	3.5	0.60
1.36	18.5	0.60	4.5	0.55	2.5	0.50
1.67	15.0	0.65	3.0	0.60	2.0	0.45
1.94	11.5	0.55	2.5	0.60	1.5	0.50
			Confined Water, $N/N_0 = 95\%$			
0.28	224.0	0.80	120.5	0.60	117.0	0.60
0.46	66.0	0.70	52.0	0.65	54.0	0.55
0.71	47.5	0.65	16.0	0.75	12.0	0.55
0.95	33.0	0.65	10.0	0.60	7.5	0.50
1.13	38.0	0.60	7.5	0.55	4.0	0.50
1.36	20.5	0.65	4.5	0.50	2.5	0.50
1.67	19.5	0.55	3.5	0.50	1.5	0.45
1.94	17.5	0.50	2.5	0.50	1.0	0.50
			Confined Water, $N/N_0 = 5\%$			
0.28	149.0	0.80	120.0	0.65	94.5	0.60
0.46	117.0	0.70	48.0	0.65	42.0	0.55
0.71	97.5	0.60	22.0	0.55	12.0	0.55
0.95	61.0	0.55	11.0	0.55	7.5	0.45
1.13	44.5	0.60	8.5	0.50	4.5	0.50
1.36	38.5	0.55	5.5	0.50	2.0	0.50
1.67	37.5	0.50	3.5	0.40	2.5	0.35
1.94	35.5	0.45	2.0	0.55	1.5	0.35

[a] Note that the estimated uncertainty for $\langle\tau\rangle$ values is ±0.5 and for β values it is ±0.05.

The mean relaxation time $\langle\tau\rangle$ and the width of the relaxation time distribution β are linked to the obtained HN(ω) fitting parameters τ_{HN}, α, and γ by the relation

$$\langle\tau\rangle = \left(\frac{\tau_{KWW}}{\beta}\right)\Gamma\left(\frac{1}{\beta}\right) \tag{11}$$

Γ is the Gamma function. Obviously, when, in particular, the HN(ω) shape parameters are equal to 1, the single Debye exponential time decay is restored and HN(ω) assumes the well-known Lorentzian profile.

In Figure 4 we report IQENS spectra, together with the total best fit (by eq 6) and the single components, for water in bulk and in the confined state at all the analyzed hydration percentages N/N_0, for $Q = 0.946$ Å^{-1} and $T = 20$ °C, choosing, as an example, the same spectra already reported in Figure 1.

As can be seen from a comparison of Figures 1 and 4, both CDM and RCM furnish good fits to experimental data, so at this level it is difficult to prefer a model with respect to the other.

From the fitting procedure we extracted the relevant parameters $\langle\tau\rangle$ and β, both Q dependent according to the MCT theory, that are reported in Table 3. Figure 5 shows, in a log−log plot, the behavior of the mean relaxation time $\langle\tau\rangle$ as a function of Q for all the investigated systems. As can be seen, $\langle\tau\rangle$ values tend toward high values going from picosecond to nanosecond time scale, following a power law $\langle\tau\rangle \approx Q^{-\gamma'}$. The exponent γ' tends to a value equal to 2 at higher temperatures, whereas it is equal to 2 ($\gamma' = 2$) in the case of the isotropic diffusion of bulk water. When the temperature decreases, γ' tends to become significantly less than 2, indicating a hindered and slowed diffusion as a consequence of confinement.

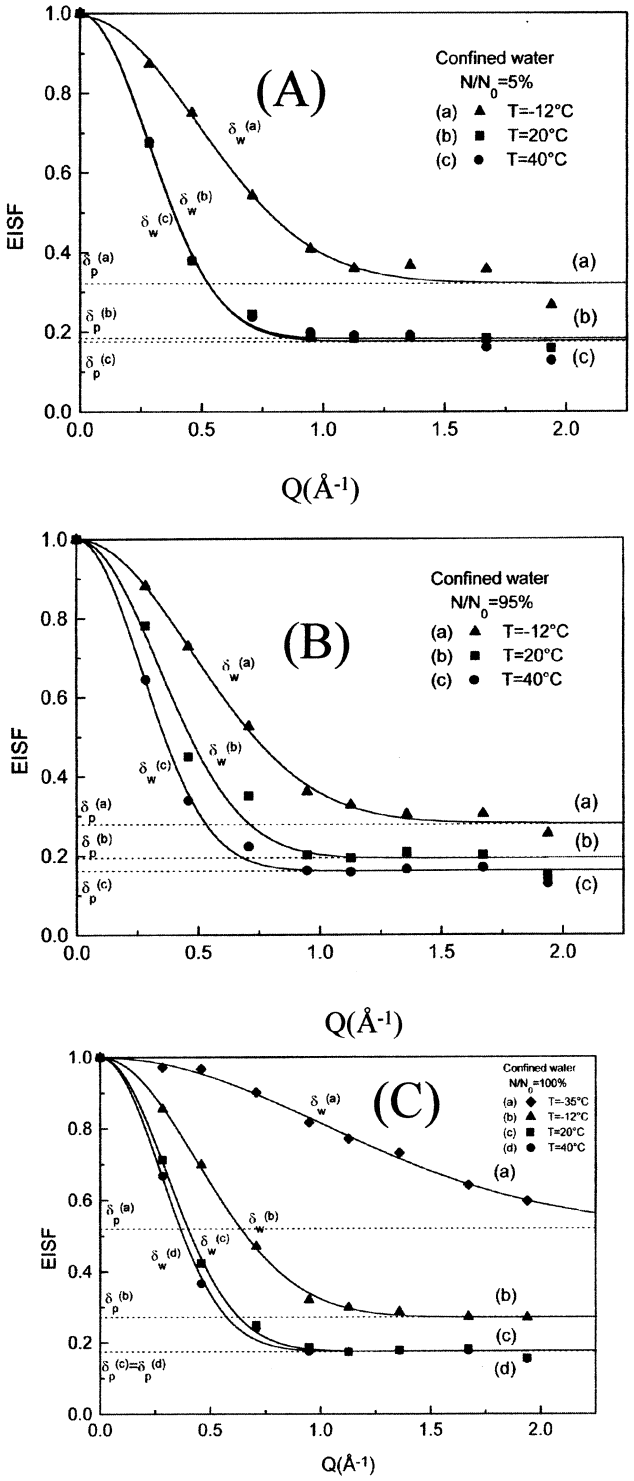

Figure 4. Experimental IQENS spectra of water in bulk (a) and in confined state at all the analyzed hydration percentages $N/N_0 = 100\%$ (b), 95% (c), and 5% (d), at $Q = 0.946$ Å^{-1} and $T = 20$ °C, together with the total best-fit and the single components. We used eq 6 to best fit the spectra, following the relaxing cage model, RCM.

The Q dependence of the stretch exponent β is reported in Figure 6 in the case of bulk water (A) at $T = 20$ and 40 °C and, as an example, for confined water at $N/N_0 = 100\%$ (B) at $T = -12$, 20, and 40 °C. β values turn out to be clearly below unity for large Q values, approaching unity for Q less than 0.1 Å^{-1}, indicating that the hydrodynamic limit is probably reached at this value. Furthermore, the observed behavior that the β values definitively increase when T diminishes can be rationalized by the occurrence of a possible transition for liquid water from a fragile (high T, low β) to strong (low T, high β) behavior.[29]

These experimental results confirm in our opinion the trend observed by other authors,[41] by means of different neutron spectrometers and using a larger pore dimension (50 Å).

(b) IINS Measurements. It is well-known that,[24] for a system of identical atoms of mass M, the one-phonon incoherent neutron differential scattering cross section can be written as

$$\frac{d^2\sigma_{inc}}{d\Omega\, d\omega} = \frac{k}{k_0} b_{inc}^{\ 2} \exp\left[-\frac{\hbar\omega}{2k_B T}\right] S(Q,\omega) \qquad (12)$$

in which $Q = k - k_0$ is the momentum transfer, $\hbar\omega$ is the energy exchange, and $S(Q,\omega)$ is the total scattering law. Introducing the reduced variables

$$\alpha = \frac{\hbar^2 Q^2}{2Mk_B T} \qquad (13)$$

and

$$\beta = \frac{\hbar\omega}{k_B T} \qquad (14)$$

and taking into account that $S(Q,\omega)$ is the total scattering law, which contains both the coherent and the incoherent scattering probabilities of the several nuclei that make up the system, we can construct the experimental generalized frequency distribution:

$$P(\alpha,\beta) = 2\beta \sinh \beta/2 \, \{S(\alpha,\beta)/\alpha\} \qquad (15)$$

The most widely used extrapolation procedure to obtain the vibrational density of states (VDOS) is due to Egelstaff[30] and Egelstaff and Schofield,[31] and consists of an extrapolation of the function P for α tending to 0. We define the experimental quantity

$$P(\beta) = \lim_{\alpha\to 0} P(\alpha,\beta) = \lim_{\alpha\to 0} 2\beta \sinh \beta/2 \, \{S(\alpha,\beta)/\alpha\} \qquad (16)$$

Since the interference part of the scattering law due to coherent scattering falls off more rapidly than the single-particle contributions for $\alpha \to 0$, $S(\alpha,\beta)$ reduces to $S_{inc}(\alpha,\beta)$, and therefore

$$P(\beta) \cong [(b_{inc}^{i})^2 + (b_{coh}^{i})^2] Z(\beta) \qquad (17)$$

where

$$Z(\beta) = 2\beta \sinh(\beta/2) \lim_{\alpha\to 0} S_{inc}(\alpha,\beta)/\alpha) \qquad (18)$$

will be the one-phonon-amplitude weighted vibrational density of states (VDOS). For liquid water $Z(\beta) \approx Z(\omega)$ becomes the VDOS connected only to the proton population.

Alternative to the procedure described above (see eqs 15−18), there is another equivalent method to obtain $Z(\omega)$, as detailed in the paper of Fontana et al.[32] In particular for an incoherent scatterer, the generalized frequency distribution $P(\alpha,\beta)$ is the Debye−Waller factor (DWF) multiplied by $Z(\omega)$, i.e., $P(\alpha,\beta) = \text{DWF} \times Z(\omega)$, assuming no multiphonon contribution and no background. Thus, we can sum over the various angles and correct for the DWF. For a coherent scatterer, the incoherent approximation is valid if the summation is done over a sufficiently large range of Q, covering the first sharp diffraction peak for a liquid or a glass. Hence we have summed

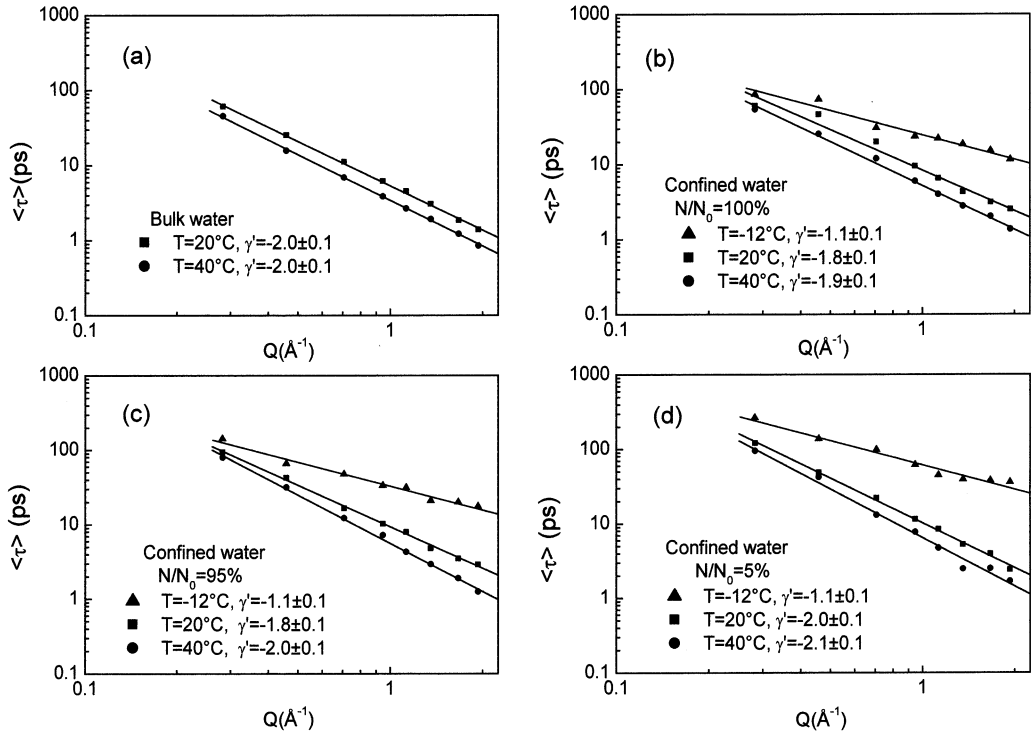

Figure 5. log−log plot of the mean relaxation times $\langle\tau\rangle$ as a function of Q for water in bulk (a) and in confined state at all the analyzed hydration percentages $N/N_0 = 100\%$ (b), 95% (c), and 5% (d), at all the studied temperatures. The continuous lines are the best fit by the power law $\langle\tau\rangle \approx Q^{-\gamma'}$; see text for details.

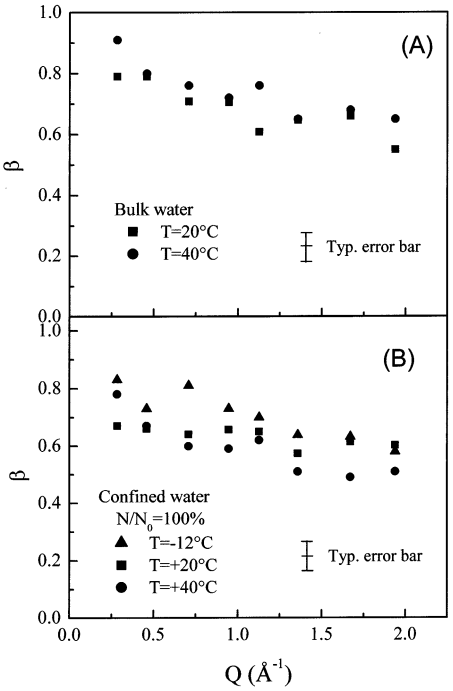

Figure 6. Q dependence of the stretch exponent β for bulk water (A), and for confined water at $N/N_0 = 100\%$ (B) at all the studied temperatures.

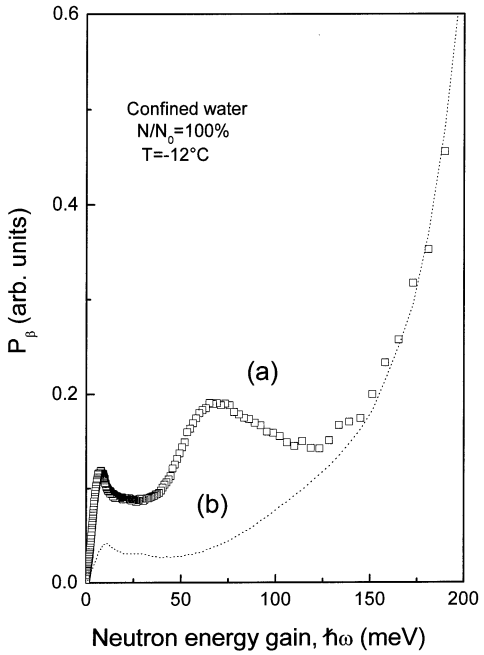

Figure 7. Experimental $P(\alpha,\beta)$ (a) for confined water at $N/N_0 = 100\%$ and $T = -12$ °C, together with the calculated multiphonon and background contributions (b).

and fitted $P(\alpha,\beta)$ with an approximate $Z(\omega)$ which allowed calculation of the DWF, multiphonon term, and background. Afterward, the multiphonon term and background were subtracted and the result was divided by the DWF, thus obtaining the experimental $Z(\omega)$.

Figure 7 shows, as an example, the experimental $P(\alpha,\beta)$ (a), in the case of confined water at $N/N_0 = 100\%$ and $T = -12$ °C, together with the calculated multiphonon and background contributions (b). For all the data reduction we used appropriate INS programs available in the ILL software library. As stressed above, we focused our attention on the evolution of $Z(\omega)$, when the water loses its peculiar bulk properties and forms a new structural environment due to its surface interactions. It is well-known that for bulk water in the low-frequency region (0−200 meV) $Z(\omega)$ shows a hindered translational spectrum convoluted with the low-frequency Debye phonon-like acoustical contribution and a librational spectrum. Both the hindered translational and rotational (librations) modes are present in water because of intermolecular bonds that give rise to the *inherent structures*

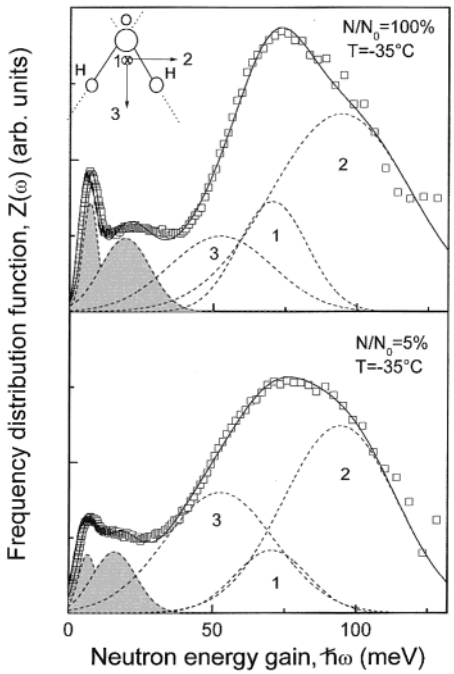

Figure 8. One-phonon proton effective VDOS for confined water at $N/N_0 = 100\%$ and 5% at $T = -35$ °C, together with the deconvoluted Gaussian components, corresponding to the two translational modes (filled area) and the three librational ones (dashed curves) around the three symmetry axes of water molecules. The inset shows the three possible symmetry axes: axis 1 perpendicular to the molecular plane, axis 2 in the molecular plane, and axis 3 the 2-fold molecular symmetry axis.

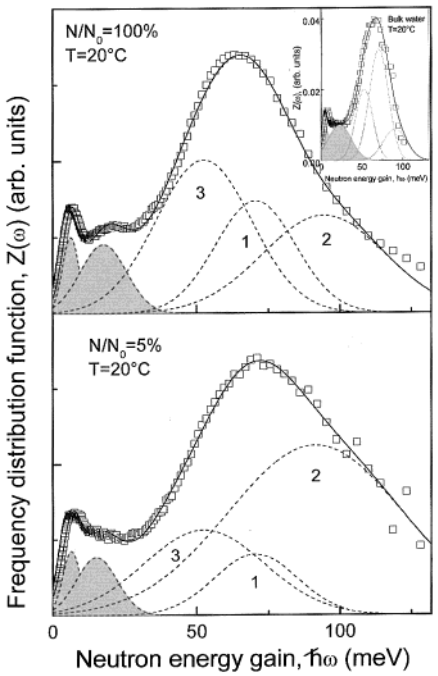

Figure 9. One-phonon proton effective VDOS for confined water at $N/N_0 = 100\%$ and 5% at $T = 20$ °C, together with the deconvoluted Gaussian components, corresponding to the two translational modes (filled area) and the three librational ones (dashed curves) around the three symmetry axes of water molecules. The inset shows the VDOS in the case of bulk water as a comparison.

of Stillinger and Weber.[33] Only when the cage relaxes (α-relaxation) do the H_2O molecules exhibit a translational and rotational diffusive contribution which does not contribute to the $Z(\omega)$ but constitutes the fine structure of the IQENS spectrum. Therefore, there is a complementary occurrence of the existence of the two hindered inelastic contributions with respect to the diffusive contribution in the water dynamics. All these features in $Z(\omega)$ are collective in character; thus it is quite natural to expect a strong spectral modification passing from bulk to confined state. Recently[18,19] it has been shown that the effects of confinement give rise to a strong modification of the translational hindered lattice bands centered at about 8 and 23 meV that are due to intermolecular tetrahedral C_{2v} symmetry, an occurrence which has been experimentally verified by IQENS[41,44] and our Rayleigh wing measurements.[18]

Following the method described in ref 32, the low-frequency portion of $Z(\omega)$ can be considered as the sum of translational $Z_T(\omega)$ and higher frequency $Z_L(\omega)$ librational bands, and because of small overlapping of the translational with the librational bands, it results[34]

$$Z(\omega) = Z_T(\omega) + M/M_L Z_L(\omega) \qquad (19)$$

where $M/M_L = M3I/2b^2$. I is the moment of inertia, b is about the O−H distance, M is the molecular mass, and M_L is an effective rotational mass. In eq 19 we have omitted the acoustical Debye-like contribution that enters in the very low-frequency part of $Z_T(\omega)$. The prefactor M/M_L is definitively higher than 1, and as a consequence, the librational bands (there are three since the symmetry axes of water molecules are three: axis 1 is perpendicular to the molecular plane, axis 2 is in the molecular plane, and axis 3 is the 2-fold molecular symmetry axis; see inset of Figure 8) are enhanced with respect to the translational ones.[35]

Figures 8 and 9 show, as an example, the evolution of $Z(\omega)$ in the case of confined water at $N/N_0 = 100\%$ and 5% at $T = -35$ °C and $T = 20$ °C, respectively. In particular, in the inset of Figure 9, the VDOS for bulk water is shown for comparison. The dashed lines are the deconvolved Gaussian bands, which are two centered at ∼8 and ∼20 meV and related to translational modes reminiscent of the two peak structures that are identifiable as the bending (60 cm^{-1}) and O···O stretching (170 cm^{-1}) intermolecular modes of water and three related to librational modes around the axes 3, 1, and 2 centered at ∼52, 70, and 91 meV. From an inspection of Figures 8 and 9, it has to be noticed that the measured and analyzed incoherent neutron spectra in confined water, generally dominated by the librational contribution, reveal (i) a flattening and attenuation of the hindered translational modes (8 and 20 meV) with respect to bulk water, indicating a strong destructuring effect in the interfacial water and (ii) enhancement, with respect to bulk water, of the librational modes having the lowest moment of inertia, centered at about 91 meV, mainly connected with the hindered rotation of water bonded with two SiOH surface groups.[16]

IV. Conclusions

In the present paper we have dealt with a detailed incoherent quasi-elastic and inelastic neutron scattering study of diffusive and vibrational dynamics of water confined in hydrophilic nanopores of a silica glass, varying the hydration level in a range between 100% (full hydration) and 5% (monolayer coverage of water molecules on the surface), and following the evolution in T from room temperature down to −35 °C.

The IQENS spectra were interpreted in terms of a confined diffusion model (CDM) and a relaxing cage model (RCM). From the data analysis the following points result:

(i) In the framework of the first model, the behavior of the half-width at half-maximum (hwhm) of the Lorentzian translational contribution shows an evident variation with Q for all

the temperatures. In particular, we revealed a flattening of hwhm to a constant value at low Q that suggests a confinement effect for the water molecules inside a restricted spatial region. The dimension of the confining region d^* was obtained by $d^* = 2\pi/Q^*$ (Q^* being the plateau wavevector) and compared with the one calculated by the fitting of the EISF term. The values turned out to be in agreement, and decrease when the temperature is lowered. This trend means that the water molecules are more localized at lower temperatures. The Q dependence of the large Q part of the quasi-elastic line width is well interpreted by a jump diffusion model, whose fitting parameters furnished the diffusion coefficients, which are lowered in the confined state.

(ii) The RCD model leads to a slow dynamics recalling the MCT relaxation process of the kinetic glass transition in dense supercooled liquids and considers the central spectral feature of the incoherent neutron scattering from interfacial water as a single quasi-elastic peak arising from a distribution of relaxation times, described by a Havriliak−Negami profile. A proper analysis of the QENS peak furnishes two important physical parameters of interfacial water: the mean relaxation time $\langle\tau\rangle$ and the width of the distribution β, both Q dependent. In particular, $\langle\tau\rangle$ values, which range from picosecond to nanosecond time scale, have a power law dependence, $\langle\tau\rangle \approx Q^{-\gamma'}$, whose exponent γ' tends to 2 when temperature increases. On the other hand, when the temperature decreases, γ' becomes significantly less than 2, indicating a hindered diffusion essentially due to the confinement effect. As far as the Q dependence of β is concerned, it turns out that the values stay below unity at large Q and definitively increase when T diminishes, indicating a possible transition for liquid water from a fragile (high T, low β) to strong (low T, high β) behavior.

Finally, as far as IINS data are concerned, the confinement effects seem to induce strongly destructive effects in interfacial water, where hydration phenomena give rise to different environments evidenced by new spectral features: a flattening and attenuation of the hindered translational modes, at about 8 and 20 meV, and an enhancement of the librational mode at about 91 meV, with respect to one observed in bulk water.

Acknowledgment. The authors thank Dr. J. Teixeira (LLB) and Dr. A. J. Dianoux (ILL) for useful discussions during the data elaboration. Furthermore, the ILL Scientific Coordination Office (SCO) is acknowledged for the dedicated beam time.

References and Notes

(1) Klafter, J.; Blumen, A.; Drake, J. M. *Relaxation and Diffusion in Restricted Geometry;* Klafter, J., Drake, J. M., Eds.; Wiley: New York, 1989.

(2) Carini, G.; Crupi, V.; D'Angelo, G.; Majolino, D.; Migliardo, P.; Mel'nichenko, Y. B. *J. Chem. Phys.* **1997**, *107*, 2292.

(3) Kremer, F.; Huwe, A.; Arndt, M.; Beherns, P.; Schwieger, W. J. *Phys.: Condens. Matter* **1999**, *11*, 175.

(4) Huwe, A.; Kremer, F.; Beherns, P.; Schwieger, W. J. *Phys. Rev. Lett.* **1999**, *82*, 2338.

(5) Arndt, M.; Stannarius, R.; Groothues, H.; Hempel, E.; Kremer, F. *Phys. Rev. Lett.* **1997**, *79*, 2077.

(6) Nemeth, Z. T.; Lowen, H. *Phys. Rev. E* **1999**, *59*, 6824.

(7) Steytler, D. C.; Dore, J. C. *Mol. Phys.* **1985**, *56*, 1001.

(8) Bellissent-Funel, M. C.; Lal, J.; Bosio, L. *J. Chem. Phys.* **1993**, *98*, 4246.

(9) Bellissent-Funel, M. C.; Sridi-Dorbez, R.; Bosio, L. *J. Chem. Phys.* **1996**, *104*, 10023.

(10) Polnazek, C. F.; Bryant, R. G. *J. Chem. Phys.* **1984**, *81*, 4038.

(11) Chen, S. H.; Bellissent-Funel, M. C.; *Hydrogen-Bond Networks;* Bellissent-Funel, M. C., Dore, J. C., Eds; NATO ASI Series C: Mathematical and Physical Science 435; Kluwer Academic: Dordrecht, 1994; p 337.

(12) Bellissent-Funel, M. C.; Chen, S. H.; Zanotti, J. M. *Phys. Rev. E* **1995**, *51*, 4558.

(13) Lynden-Bell, R. M.; Rasaiah, J. C. *J. Chem. Phys.* **1996**, *105*, 9266.

(14) Zhu, S. B.; Robinson, G. W. *J. Chem. Phys.* **1991**, *94*, 1403.

(15) Gallo, P.; Rovere, M.; Spohr, E. *Phys. Rev. Lett.* **2000**, *85*, 4317.

(16) Steytler, D. C.; Dore, J. C.; Wright, C. J. *Mol. Phys.* **1983**, *48*, 1031.

(17) Spohr, E.; Hartnig, C.; Gallo, P.; Rovere, M. *J. Mol. Liq.* **1999**, *80*, 165. Gallo, P.; Rovere, M.; Ricci, M. A.; Hartnig, C.; Spohr, E. *Philos. Mag. B* **1999**, *79*, 1923.

(18) Crupi, V.; Magazù, S.; Majolino, D.; Maisano, G.; Migliardo, P. *J. Mol. Liq.* **1999**, *80*, 133. See also: Crupi, V. S.; Majolino, D.;.; Migliardo, P.; Venuti, V. *J. Phys. Chem. A* **2000**, *104*, 11000.

(19) Zanotti, J. M.; Bellissent-Funel, M. C.; Chen, S. H. *Phys. Rev. E* **1999**, *59*, 3084.

(20) Volino, F.; Dianoux, A. J. *Mol. Phys.* **1980**, *41*, 271.

(21) Leuthesser, E. *Phys. Rev. A* **1984**, *29*, 2765. Bengtzelius, U.; Gotze, W.; Sjolander, A. *J. Phys. C* **1984**, *17*, 5915.

(22) Crupi, V.; Dianoux, A. J.; Majolino, D.; Migliardo, P.; Venuti, V. *Phys. Chem. Chem. Phys.* **2002**, *6*, 2768. See also: Crupi, V.; Majolino, D.; Migliardo, P.; Venuti V. *Appl. Phys. A* **2002**, *74*, in press.

(23) Carini, G.; Crupi, V.; D'Angelo, G.; Majolino, D.; Migliardo, P.; Mel'nikenko, Yu. *J. Chem. Phys.* **1997**, *107*, 2292.

(24) Marshall, W. and Lovesey, S. *Theory of Thermal Neutron Scattering;* Oxford University Press: London, 1971.

(25) Teixeira, J.; Bellissent-Funel, M. C.; Chen, S. H.; Dianoux, J. A. *Phys. Rev. A* **1985**, *31*, 1913.

(26) Bee, M. *Quasielastic Neutron Scattering*; Hilger, A., Ed.; Philadelphia and Bristol Press, 1988; Chapter 9, p 357.

(27) Debenedetti, P. G.; Stillinger, F. H. *Nature* **2001**, *410*, 259.

(28) Alvarez, F.; Alegria, A.; Colmenero, J.; Alberdi, J. M.; Frick, B. *Phys. Rev. B* **1991**, *44*, 7321. See also: Alvarez, F.; Alegria, A.; Colmenero, J.; *Phys. Rev. B* **1991**, *44*, 7306.

(29) Ito, K.; Moyniham, C. T.; Angell, C. A. *Nature* **1999**, *389*, 492.

(30) Egelstaff, P. A. *IAEA Proceedings*; IAEA: Vienna, 1961.

(31) Egelstaff, P. A.; Schofield, P. *Nucl. Sci. Eng.* **1962**, *12*, 260.

(32) Fontana, A.; Rocca, F.; Fontana, M. P.; Rosi, B.; Dianoux, A. J. *Phys. Rev. B* **1990**, *41*, 3778.

(33) Aliotta, F.; Vasi, C.; Maisano, G.; Majolino, D.; Mallamace, F.; Migliardo, P. *J. Chem. Phys.* **1986**, *84*, 4731.

(34) Prask, H.; Boutin, H.; Yip, S. *J. Chem. Phys.* **1968**, *48*, 3367.

(35) Rahman, A.; Stillinger, F. H. *J. Chem. Phys.* **1971**, *55*, 3336.